



respectively. Later a dual fuel thrust augmented nozzle engine was designed and tested, which took into account the problem of incomplete combustion. The thrust increment was over forty percentage (Forde *et al.* 2006; Bulman 2009). The secondary injection introduces additional mass, momentum and energy to the expanding main flow. This also reduces the effective area at the exit of the nozzle; thus giving a better thrust to the rocket at the initial stage of take off, when the nozzle is otherwise over expanded (Forde *et al.* 2006). Even though TAN is a simple design, the flow features are rather complex and involve different types of shocks due to the sudden blockage of the supersonic main flow. Therefore, it is always interesting to study simpler test cases before proceeding in to the actual TAN design. A secondary injection on a flat plate is one such test case of interest, which is sometimes called jet in cross flow (JICF) (Margason, 1993; Santiago & Dutton 1997). The only difference of TAN from JICF is the expanding supersonic flow and the associated pressure drop. The flow features and physics associated with JICF are similar to TAN, and could be easily compared.

The first available detailed experimentation and inferences in the field of sonic jet issuing into a supersonic flow were given by Spaid and Zukoski (1964). An analogy between the transverse jet and a solid body of a particular length and shape in non-viscous flows was made in the study. The paper presented an analytical model for the flow features involved. However, this simplistic model was not capable of predicting plume over expansion, vortex generation and separation topology. Later, Young and Barfield (1971) presented another analytical study where the alteration of a two-dimensional flow field due to a secondary sonic injection was presented. Studies conducted by Fuller *et al.* (1991) used the ratio of jet momentum flux to the free stream as the principal controlling parameter for obtaining an optimum penetration. While Schetz and Billig (1966) suggested that optimum penetration happens for a normally injected sonic jet when the static pressure of the jet is equal to the effective back pressure. Fuller *et al.* (1992) found out that the mixing efficiency is dramatically affected when the free stream Mach number is very high (Mach 6).

A more relevant study in this regard was done by Aso, where the influence of a sonic slot injection (Aso *et al.* 1991) and circular injection (Aso *et al.* 1994) to a supersonic flow over a flat plate was studied. The study was about the expansion of the injected jet, when it enters into the main supersonic flow. The complex flow features like the Mach disc, barrel shock, separation shock and the re-compression shock were also studied. The interpretation was that the bow shock is formed due to sudden blockage of the high-speed main flow by the sonic injection. The flow physics helps to understand the general phenomena involved in JICF better, and bring out a comparison between hot flow and cold flow studies. For example, the behavior of the counter rotating vortex pairs in a turbulent reactive flow were studied by Karagozian (1986) to understand the entrainment of the oxidizer by the

fuel jet.

Rizzetta (1992) numerically validated the experimental studies of Aso. He used an explicit time dependent finite difference algorithm (MacCormack) with Lauender  $k-\epsilon$  turbulence modeling. Simulations, which are in better agreement with experimental results of wall pressure distribution in both upstream and downstream of the jet was conducted by Sriram and Mathew (2008). A finite volume Roe solver with Wilcox  $k-\omega$  turbulence modeling was used for this Riemann problem. In the study, semi-implicit Runge Kutta method was adopted for time stepping. For the present study, the SST turbulence model (Menter, 1993), which utilizes the advantage of both  $k-\epsilon$  and  $k-\omega$  models is used.

Even though there are several experimental and numerical studies conducted on JICF, there is a lack of understanding in the intricacies of secondary injection into an expanding supersonic flow. The objective of this work is to get a theoretical understanding of the JICF phenomenon for a supersonic flow from a simple flat plate injection and extending it to an expanding supersonic flow. The simulation study conducted by Shyji *et al.* (2017) is used as a reference for understanding the salient flow features in a diverging nozzle. To understand the flow features and performance parameters, the methodology adopted in the present study involves experimental and numerical approaches. Experimental studies are conducted to obtain the wall pressure data and shock features at different locations. The wall pressure distribution and Schlieren images are compared with the numerical results. Conclusions are made based on the previous studies on JICF and present results.

## 2. METHODOLOGY

### 2.1. Experimental Approach

Experimental study is conducted at the supersonic free jet facility of Advanced Propulsion and Laser Diagnostic Laboratory (APLD) in IIST, Thiruvananthapuram. The free jet facility consists of an ELGI<sup>TM</sup> (Model: E18-10) single-stage air cooled screw compressor, a GEM<sup>TM</sup> air-dryer, a reservoir tank with a pressure storage capacity of 12 bar as shown in Figure 1. The stagnation temperature is assumed to be 300K and all the pressures are absolute. Controlled flow of air inside the test section is done by PID controller. Pressure measurements are required at the wall surface of the expanding nozzle and this is done by unsteady transducers.

Kulite<sup>TM</sup> (Model: XCQ-152 Series) transducers are used for the pressure measurements. The locations of transducers are shown in Fig. 2.

Three nozzle configurations (2D) are manufactured, in which slots were cut in two of them to give angled injections of  $15^\circ$  and  $30^\circ$  with respect to the tangent of the nozzle contour. The nozzle is designed to produce an exit Mach number of 2, using the

method of characteristics. The injector slot width is 1 mm. The detailed dimensions of the nozzle will be discussed in the next subsection. For each nozzle configurations, three sets of experiments are conducted for cross flow absolute pressures of 3 bar, 4 bar and 5 bar. For the injections cases, the pressures at the injector were 2 bar and 3 bar absolute. Unsteady pressure transducers are used to measure the pressure at different locations (Fig. 2). Additionally Schlieren images were taken with a Pixelfly camera (make PCO) with 1392×1040 resolution and 14 bit dynamic range.

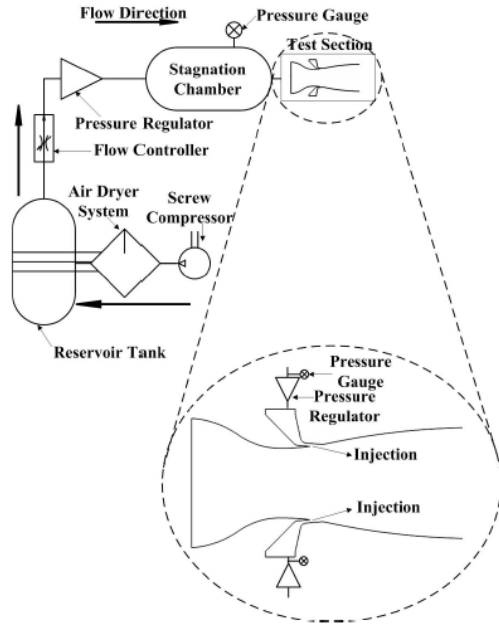


**Fig. 1. Layout of the experimental facility.**

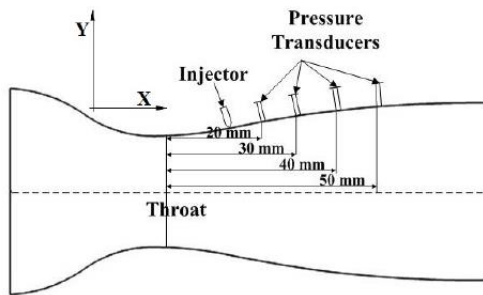


**Fig. 2. Location of the pressure transducers.**

Experiments were conducted on different operating conditions. Table 1 shows the operating conditions adopted and terminology used for different configurations. For a nozzle with no injection, the number at the end in the terminology denotes the cross flow stagnation pressure. For example NoInj\_3 means the cross flow stagnation pressure used is of 3 bar. For injection cases, the first number denotes the injection angle, the second number denotes the cross flow stagnation pressure and the third number denotes the injection pressure. For example 15\_3CF\_2Inj means the cross flow stagnation pressure is 3 bar, and injection is given at an angle of

15° and 2 bar.

**Table 1 Operating Conditions and Terminology**

Nozzle Config.	Exp. Conditions		Terminology
	Cross Flow Stagnation Pressure (bar)	Injection Pressure (bar)	
No Injection	3	-	NoInj_3
	4	-	NoInj_4
	5	-	NoInj_5
15°	3	2	15_3CF_2Inj
	3	3	15_3CF_3Inj
	4	2	15_4CF_2Inj
	4	3	15_4CF_3Inj
	5	2	15_5CF_2Inj
30°	3	2	30_3CF_2Inj
	3	3	30_3CF_3Inj
	4	2	30_4CF_2Inj
	4	3	30_4CF_3Inj
	5	2	30_5CF_2Inj
	5	3	30_5CF_3Inj

## 2.2. Computational Approach

### 2.2.1. Governing Equations

The two dimensional Navier-Stokes equation for solving compressible turbulent flows is given as follows:

$$\frac{\partial U}{\partial t} + \frac{\partial(F - F_v)}{\partial x} + \frac{\partial(G - G_v)}{\partial y} = S \quad (1)$$

The vector of conservation variables is defined as

$$U = [\rho, \rho u, \rho E, \rho k, \rho \varepsilon]^T \quad (2)$$

The flux vectors for the two Cartesian directions are given by

$$F = [\rho u, \rho u^2 + P, \rho uv, (\rho E + P)u, \rho uk, \rho u \varepsilon]^T \quad (3)$$

$$G = [\rho v, \rho vu, \rho v^2 + P, (\rho E + P)v, \rho vk, \rho v \varepsilon]^T \quad (4)$$

Viscous flux vectors are given as

$$F_v = [0, \tau_{xx}, \tau_{xy}, Q_x, \mu_k \frac{\partial u}{\partial x}, \mu_\varepsilon \frac{\partial \varepsilon}{\partial x}]^T \quad (5)$$

$$G_v = [0, \tau_{xy}, \tau_{yy}, Q_y, \mu_k \frac{\partial v}{\partial y}, \mu_\varepsilon \frac{\partial \varepsilon}{\partial y}]^T \quad (6)$$

Where,

$$Q_x = u\tau_{xx} + v\tau_{xy} + k \frac{\partial T}{\partial x} \quad (7)$$

$$Q_y = u\tau_{xy} + v\tau_{yy} + k \frac{\partial T}{\partial y} \quad (8)$$

In the above equation, the stress terms are given as

$$\tau_{xx} = (\lambda + 2\mu) \frac{\partial u}{\partial x} + \lambda \frac{\partial v}{\partial y} \quad (9)$$

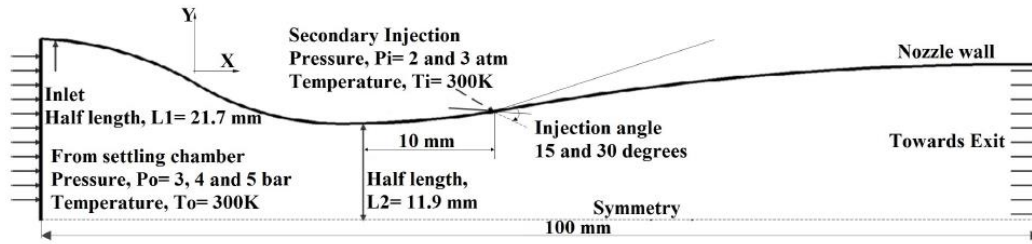


Fig. 3. Computational domain and boundary conditions used for the simulation

$$\tau_{xy} = \mu \left( \frac{\partial u}{\partial y} + \frac{\partial v}{\partial x} \right) \quad (10)$$

$$\tau_{yy} = (\lambda + 2\mu) \frac{\partial v}{\partial y} + \lambda \frac{\partial u}{\partial x} \quad (11)$$

where  $u$  and  $v$  are the velocities in the  $x$  and  $y$  directions respectively,  $\rho$  is the density,  $E$  is the total energy and  $k$  is the thermal conductivity. In the above equations, the coefficient of viscosities are related as follows

$$\lambda = -\frac{2\mu}{3} \quad (12)$$

The source term in the right hand side of equation (1) is given by

$$S = [0, 0, 0, 0, H_k, H_\varepsilon]^T \quad (13)$$

The pressure,  $P$  for an ideal gas is calculated as follows:

$$P = \rho RT \quad (14)$$

where  $R$  is the universal gas constant and  $T$  is the static temperature.

### 2.2.2. Numerical Method

The density based Harten Lax-Van Leer-Contact (HLLC) Riemann solver (Harten *et al.* 2011) available in Metacomp Technologies' CFD++ is used for the simulations in the present work. This commercial package is well validated and widely used for supersonic flow computations (Metacomp, 2015). An implicit time integration of CFD++ is chosen for the simulations and the local Courant number is ramped from 1 to 5 using the automatic Courant number adjustment procedure (ADAP), for the first 100 iterations. Simulations are run till the normalized residuals of mass, momentum and energy are dropped below  $10^{-5}$ . Steady state RANS (Reynolds Averaged Navier Stokes Equation) simulations are done with Shear Stress Transport (SST) turbulence modeling. The geometry used and the boundary conditions imposed are shown in Figure 3.

### 2.3. Validation Study

The validation study for the numerical method is done based on the results published by Aso *et al.* (1991), for a sonic slot injection to a supersonic cross flow. Figure 4 shows the normalized wall pressure

( $P / P_\infty$ ) distribution (where  $P$  is the absolute static pressure on the surface of the wall and  $P_\infty$  is the free stream static pressure of the flow). For the normalized  $x$  direction ( $X / X_{ref}$ ),  $X_{ref}$  denotes the location of the injector. The results are compared with the experimental result of Aso *et al.* (1991) and the numerical result of Rizzetta (1992).

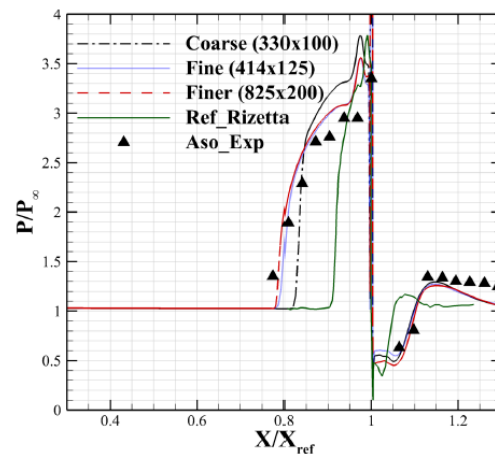


Fig. 4. Wall pressure distribution on a flat plate.

Simulations were conducted for two different static pressure ratios ( $P_{injector} / P_{freestream}$ ) - 0.49 and 0.085. It is to be noted that here only the injector pressure ( $P_{injector}$ ) is varied keeping the free stream pressure a constant value of 21 bar. The inlet condition is maintained at a temperature (stagnation) of 300 K. A sonic boundary condition is given at the injector maintaining a static temperature of 80 K and varying pressures. The fluid in the free stream is assumed to be air and in the injector to be Nitrogen ( $N_2$ ). A supersonic out flow boundary condition is given at the right end of the domain and a free slip condition is given at the top of the domain. The bottom part of the domain is a viscous wall. The validation results have enabled to confirm the numerical method and turbulence modeling required for the present study on jet injection in to a nozzle divergence.

### 2.4. Grid convergence Study on the Supersonic Nozzle

For the grid independence study, three meshes with

7155 cells (coarse), 15245 (medium) and 22346 (fine) cells are made. The  $y^+$  of 1 is used and consequently the wall spacing of the first cell ( $\Delta s$ ) was found out to be  $3.5 \times 10^{-4}$  mm. For capturing high gradients near the injector, the density of the grid is increased in this region as well. Different chamber stagnation pressures of 3 bar, 4 bar and 5 bar were given at the nozzle inlet with a stagnation temperature of 300 K. Atmospheric pressure of 1.01 bar was imposed at the outlet. Wall pressure distribution is chosen as the local parameter for the grid independence. The study is done on  $15^\circ$  angle of injection grid with 2 bar injection and 3 bar cross flow pressures. A good match is obtained for two grids after successive refinement as shown in Figure 5. The simulation results are also compared with the experimental results with same conditions. Thrust, being an integrated parameter relevant for this study, is also considered for the grid independence study. Table 2 shows the variation of thrust for different mesh types. Mesh size corresponding to the second level of refinement (medium) has been chosen for the remaining simulations.

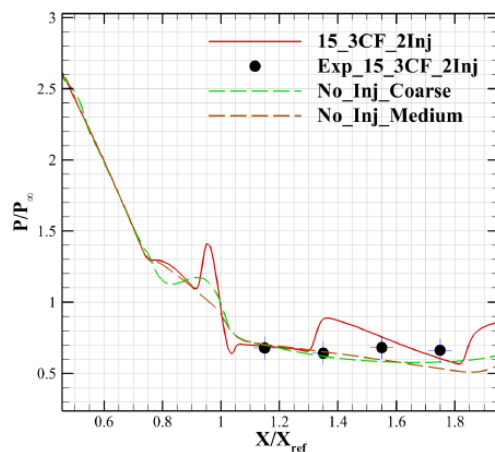


Fig. 5. Grid independence- Wall pressure distribution in the nozzle.

Table 2 Thrust for different mesh types

Mesh type	Thrust, $N$
coarse (7155 cells)	210
medium (15245 cells)	229
fine (22346 cells)	233

### 3. RESULTS AND DISCUSSION

#### 3.1. Physics of the Flow

The nature of flow features and shock interactions are well understood for a jet issuing into a free stream supersonic flow and an expanding supersonic flow (Shyji *et al.* 2017; Candon & Ogawa 2015). Figures 6 and 7 show the experimental and numerical schlieren images for the conditions 15\_4CF\_2Inj and 30\_3CF\_2Inj (see Table 1). The obstruction of the main flow by the secondary injection leads to a bow shock and this become very weak when the injection pressure is very low. It is observed from the present

study that the strength of this shock is further reduced when the secondary injection is at angles  $15^\circ$  and  $30^\circ$ . Consequently all the associated features like the separation shock, recompression shock and the jet induced shock become weak. The upstream vortices are non-existent for a lower angle of injection and lower pressure. In the present study, upstream and downstream vortices are seen only for the case in which the angle of injection is  $30^\circ$  (see Fig. 7).

#### 3.2. Comparison of Wall Pressure Distribution

Experimental and numerical values of wall pressure normalized distribution with respect to atmospheric pressure for different cases are plotted against the X-axis normalized with respect to injector location (Figs. 8a- 8d). From the figures it is evident that there is a close agreement between the experimental and simulation wall pressure distribution. A trend observed in general is the existence of the weak reflected shock earlier (upstream) in the simulation results (see Figs. 6 and 7 as well). This shows that that angle of the separation shock with respect to the X-axis is slightly higher in the simulation as compared to the experimental studies. The strength of this shock is also slightly higher in the simulations  $15^\circ$  angle of injection case. The strength is more or less the same when the injection angle is  $30^\circ$ . Existence of a strong oblique shock at the exit for lower cross flow pressures could also be confirmed because of the sudden shoot of wall pressure here.

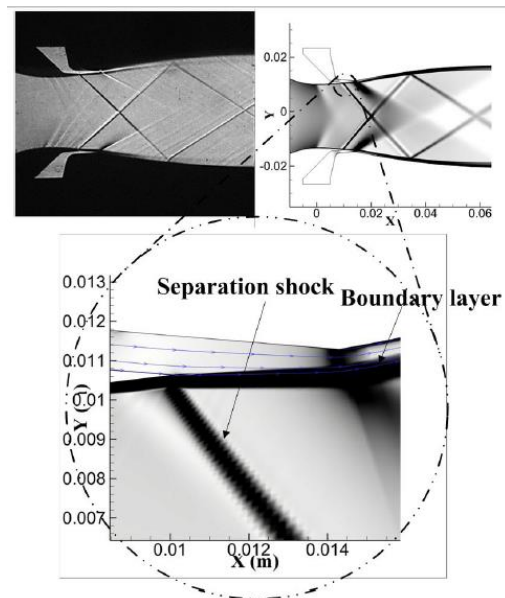
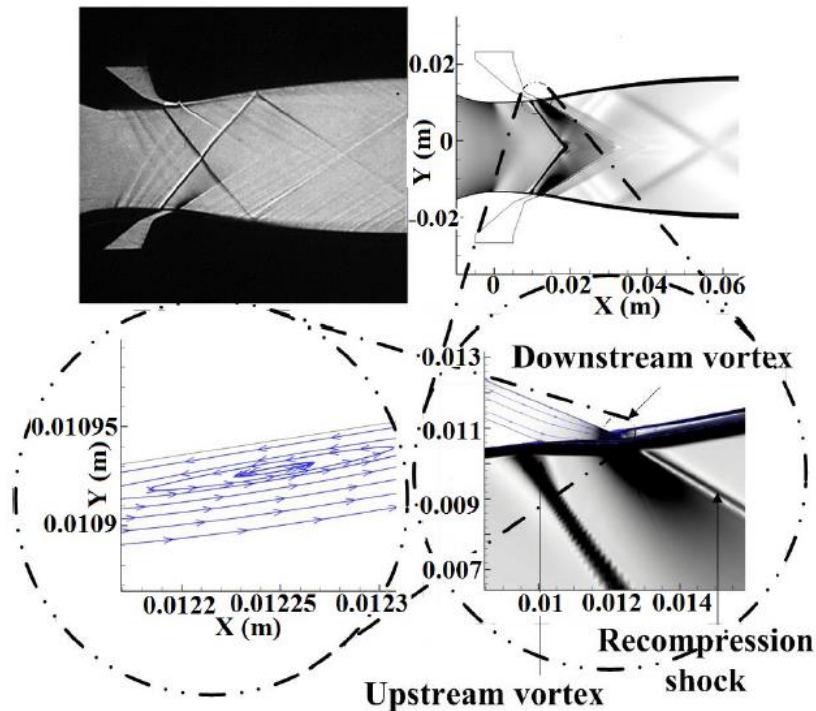


Fig. 6. Schlieren images for  $15^\circ$  injection- experimental (top left) and numerical (top right). Separation region is zoomed in the image.

#### 3.3. Effect of Injection Pressure on the flow Field

It is found that, as the injection pressure increases, the start of the peak at the upstream further travels



**Fig. 7.** Schlieren images for  $30^\circ$  injection- experimental (top left) and numerical (top right). Presence of vortices in separated zone is shown in zoomed images.

upstream and intuitively the peak at the injector is also increased. The upstream traveling of the start of the separation shock at the upstream for a higher pressure ratio. At the downstream of the injector, there is a sudden decline followed by a surge of the wall pressure distribution. The pressure drop denotes the formation of vortices at the immediate downstream and the static pressure surge denotes the recompression shock at that location (See Fig. 4). For a higher pressure ratio (Figure 8b and 8d) case the recompression shock occurs later as compared to the low pressure ratio (Figs. 8a and 8c) case. The penetration height in the figure is understood by the pressure peak at the injection location ( $X / X_i = 1$ ). This was observed in the study of Aso *et al.* as well. He observed that there is a linear relationship between pressure ratio and penetration height for a constant slot width up to a certain pressure ratio, beyond which the behavior is non-linear.

### 3.4. Effect of Injection Conditions on Nozzle Flow Fields

The decrease in pressure towards the exit of the nozzle with increasing Mach number is typical for an isentropic expansion process. This nozzle with no injection is designed to give an exit Mach number of 2 for a given pressure ratio. A suitable pressure ratio should be chosen, so that there is no under or over expansion; because in either cases, there will be a considerable loss of thrust. As stated earlier, the chamber temperature is assumed to be 300 K. Even though, it is the actual temperature in the pressure chamber for the experimental set-up, the temperature

is not realistic for a functional nozzle.

From the Mach number contours (Fig. 9), it is clear that a sonic injection is not attained at the injector exit in many test conditions. This is due to low  $P_{injector} / P_{freestream}$ . The figure shows the Mach contours for 4 bar cross flow pressure. For higher cross flow pressure, the injection is given at a point where the nozzle is not expanded enough to give a considerable pressure ratio difference ( $P_{injector} / P_{freestream}$ ). This may reduce the effective thrust but not to a great extent since the presence of shocks affects the pressure component of thrust at the exit, which has only a small contribution to the total thrust of an ideally expanded nozzle (which will be discussed in more detail in the next section).

### 3.5. Performance Comparisons: Thrust

Thrust ( $T$ ) is calculated as follows:

$$T = \dot{m} \times V_e + (P_e - P_a) \times A_e \quad (15)$$

where  $\dot{m}$  is the mass flow rate,  $V_e$  is the exit velocity,  $P_e$  is the exit pressure and  $P_a$  is the ambient pressure. Subsequently, the thrust coefficient ( $C_f$ ) is calculated as follows:

$$C_f = T / (A^* \times P_o) \quad (16)$$

where  $A^*$  is the throat area  $P_o$  is the chamber pressure (cross flow pressure). The thrust coefficients are calculated at nineteen different axial planes just after the injection. Figure 10 shows the

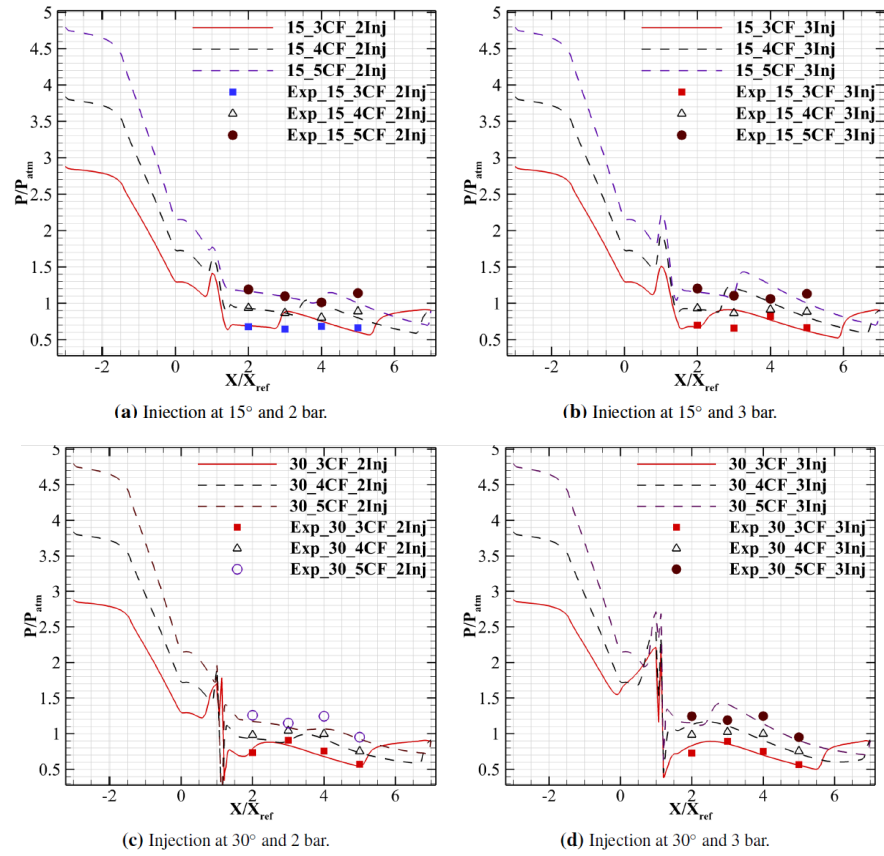


**Fig. 8. Comparison of wall pressure distribution.**

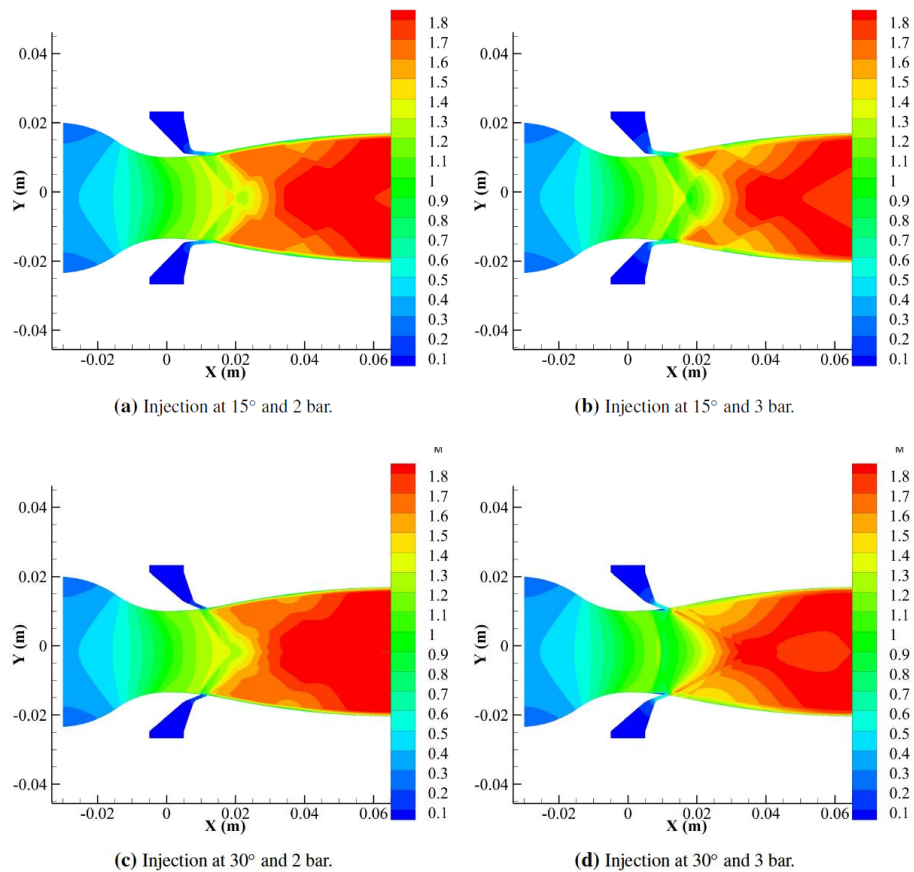


**Fig. 9. Mach number contours for a nozzle with 4 bar cross flow stagnation pressure.**

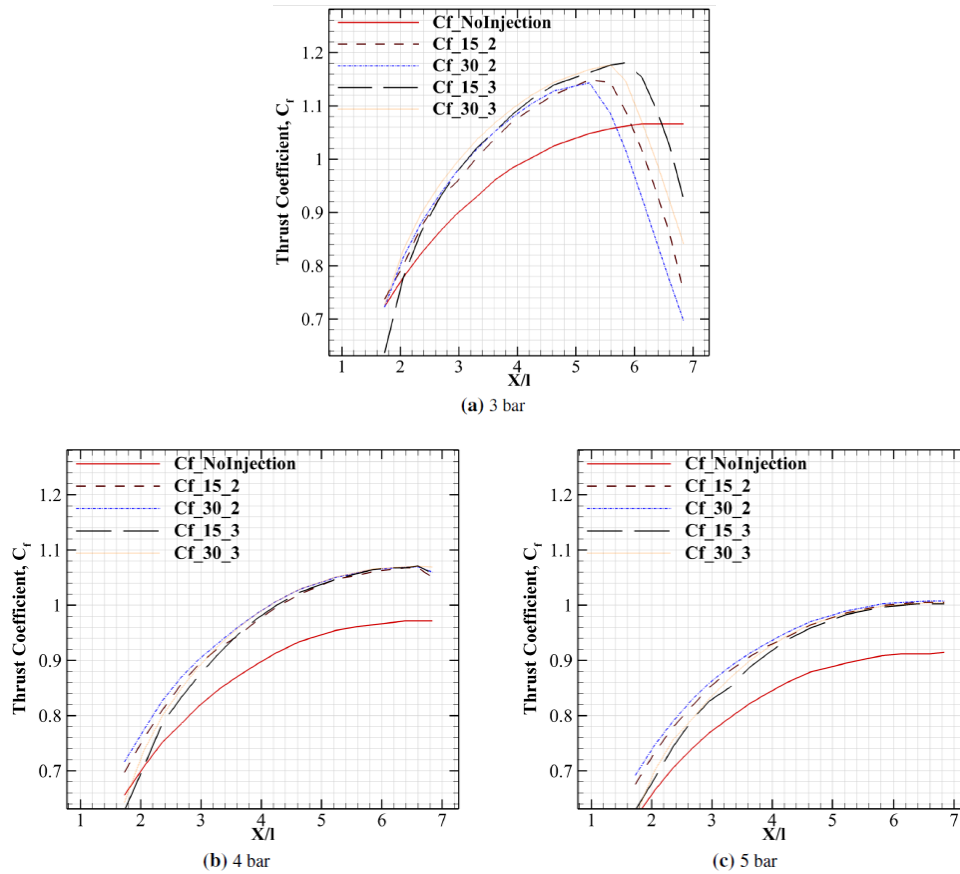


**Fig. 10. Thrust coefficient variation for different cross flow stagnation pressures.**

variation of thrust coefficient along the X-axis normalized with respect to the injection location. The variation along X-axis is relevant because of the change in area ratio as we move along this axis. Thus, this graph could be interpreted as the variation of thrust for an increasing area ratio for different angles of injection. In these figures the first and second number represents the injection angle (degrees) and injection pressure (bar) respectively. For example Cf<sub>15\_2</sub> means the thrust coefficient for an injection angle and pressure of 15° and 2 bar respectively. It could be concluded that for the present cold flow study, where there is no reaction involved, there is a good increase (over 11 percentage for 5 bar cross flow) in thrust when there is a secondary injection. The thrust coefficient also gives a picture of amplification of thrust due to the nozzle.

Table 4 shows the total thrust given by the nozzle at different injection and cross flow conditions. From Figures 10 and Table 4, it is clear that there is a positive correlation between the cross flow pressure and thrust, but the cross flow pressure required for optimum thrust for this particular nozzle should be between 3 and 5 bar. The advantage of secondary injection is also more clearly seen for the lowest cross flow pressure (3 bar), where a nozzle with lower expansion ratio could be used for better effective thrust as suggested by the peaks of injection cases in Figure 10a. The start of flow separation and

associated adverse pressure gradient for a 3 bar cross flow condition is well seen in Figs. 8a- 8d (after  $X / X_{ref} = 5$ ). It can be seen that, there is a sudden drop in thrust value, when the cross flow stagnation pressure is 3 bar at this point (corresponding point in Figure 10a is approximately  $X/l = 5$ ). This is due to over expansion and predicates that a further expansion of the nozzle beyond this particular area ratio doesn't give an advantage for thrust augmentation.

It is found out that, there is an overall increase in thrust when there is secondary injection. From the current studies, it is also worth noting that when the pressure ratio ( $P_{injector} / P_{freestream}$ ) is small, there is a positive correlation between injection pressure and thrust value. For higher cross flow pressure, there is no advantage in increasing the injection pressure for a particular nozzle (see Table 4). Maximum thrust coefficient augmentation of 11.11 % is attained for the 5 bar cross flow condition, followed by 10.25 % for 4 bar cross flow condition.

Major losses are encountered due to the separation of exhaust gases from a high area ratio nozzle for a particular cross flow pressure (Bulman, 2006). Secondary injection is not always advantageous in increasing the thrust, for example when the cross flow pressure is low, as seen in figure 10a. There is a trade-off among the two factors (momentum and pressure) that contribute the thrust for various angles

of injection. Though secondary injection contributes positively towards the thrust available at exit, increased shock losses in nozzle flows adversely affect the same.

**Table 4 Effective thrust for different nozzles**

Injection angle	Injection pressure, bar	Cross flow pressure, bar	Thrust, N
No injection	-	3	233
	-	4	283
	-	5	333
15°	2	3	164
	3	3	202
	2	4	306
	3	4	308
	2	5	366
	3	5	365
30°	2	3	152
	3	3	184
	2	4	308
	3	4	312
	2	5	367
	3	5	366

#### 4. CONCLUSION

In this study on thrust augmentations of a rocket nozzle, validation studies on the effects of secondary injection on both expanding and non expanding supersonic flows was made. The physics of the flow is compared for both cases. There is an increase in wall static pressure due to secondary injection and has a positive correlation with injection pressure. Thrust augmentation is attained, when there is secondary injection. It could be concluded that, when the chamber pressure is sufficiently high, there is a thrust augmentation due to secondary injection. The maximum augmentation percentage is obtained for the highest cross flow pressure used in the present study. It is also found that secondary injection is also beneficial to delay the flow separation near the exit of the nozzle due to the formation of oblique shocks. For preventing the over-expansion in the nozzle, a proper injection pressure and angle could be adopted.

#### REFERENCES

Aso, S., M. Tannou, S. Maekawa, S. Okuyama, Y. Ando, Y. Yamane and M. Fukuda (1994). A Study on Mixing Phenomena in Three-Dimensional Supersonic Flow with Circular Injection. In *32nd Aerospace Sciences Meeting & Exhibit proceedings*, Volume 94, Reno. American Institute of Aeronautics and Astronautics.

Aso, S., S. Okuyama, M. Kawai, Y. And and I. Co (1991). Experimental Study on Mixing Phenomena in Supersonic Flows With Slot Injection. In *29th Aerospace Sciences Meeting proceedings*, Volume 91, Reno. American Institute of Aeronautics and Astronautics.

Bulman, M. J. (2006). Thrust Augmented Nozzle ( TAN ): The New Paradigm for Booster Rockets. In *AIAA/ASME/SAE/ASEE Joint Propulsion Conference & Exhibit proceedings*, Volume 42, pp. 1–8.

Bulman, M. J. (2009). Variable Element Launcher. In *AIAA/ASME/SAE/ASEE Joint Propulsion Conference & Exhibit proceedings*, Denver, Colorado, pp. 1–13.

Candon, M. J. and H. Ogawa (2015). Thrust augmentation optimization through supersonic after-burning in scramjet engine nozzles via surrogate-assisted evolutionary algorithms. *Acta Astronautica* 116, 132–147.

Flamm, J., K. Deere, M. Mason, B. Berrier and S. Johnson (2006). Design Enhancements of the Two-Dimensional, Dual Throat Fluidic Thrust Vectoring Nozzle Concept. In *3rd AIAA Flow Control Conference proceedings*, San Francisco, California, pp. 1–27. American Institute of Aeronautics and Astronautics.

Forde, S., M. Bulman and T. Neill (2006). Thrust augmentation nozzle (TAN) concept for rocket engine booster applications. *Acta Astronautica* 59(1-5), 271–277.

Fuller, E. J., R. B. Mays, R. H. Thomas and J. A. Schetz (1992). Mixing studies of he-lium in air at high supersonic speeds. *AIAA Journal* 30(9), 2234–2243.

Fuller, E. J., R. Thomas and J. Schetz (1991). Mixing studies of helium in air at Mach 6. In *27th Joint Propulsion Conference*, pp. 1–15. AIAA Paper.

Harten, A., P. D. Lax and B. Van Leer (2011). On Upstream Differencing and Godunov-Type Schemes for Hyperbolic Conservation Laws. *SIAM REVIEW* 25(1), 35–61.

Karagozian, A. R. (1986). The flame structure and vorticity generated by a chemically re-acting transverse jet. *AIAA Journal* 24(9), 1502–1507.

Margason, R. J. (1993). Fifty years of jet in cross flow research. In *Proceedings of the AGARD Symposium on Computational and Experimental Assessment of Jets in Crossflow*, Volume 1, Winchester, UK, pp. 1–41.

Menter, F. R. (1993). Zonal Two Equation k-omega Turbulence Models for Aerodynamic Flows. In *24th Fluid Dynamics Conference proceedings*, Volume 93-2906, Orlando, Florida, pp. 1–21. American Institute of Aeronautics and Astronautics 370.

Metacomp (2015). *CFD++ User manual*, Metacomp Technologies, CA, USA.

Rizzetta, D. (1992). Numerical simulation of slot injection into a turbulent supersonic stream. *AIAA Journal* 30(10), 2434–2439.

Santiago, J. G. and J. C. Dutton (1997). Velocity Measurements of a Jet Injected into a Supersonic Crossflow. *Journal of Propulsion and Power* 13(2), 264–273.

- Schetz, J. A. and F. S. Billig (1966). Penetration of gaseous jets injected into a supersonic stream. *Journal of Spacecraft and Rockets* 3(11), 1658–1665.
- Shyji, S., M. Deepu, N. A. Kumar and T. Jayachandran (2017). Numerical studies on thrust augmentation in high area ratio rocket nozzles by Secondary injection. *Journal of Applied Fluid Mechanics* 10(6), 1605–1614.
- Spaid, F. W. and E. Zukoski (1964). Secondary injection of gases into a supersonic flow. *AIAA Journal* 2(10), 1689–1696.
- Sriram, A. T. and J. Mathew (2008). Numerical Simulation of Transverse Injection of Circular Jets into Turbulent Supersonic Streams. *Journal of Propulsion and Power* 24(1), 45–54.
- Young, C. C. and B. F. Barfield (1971). Viscous Interaction of Sonic Transverse Jets with Supersonic External Flows. *AIAA Journal* 9(2), 304–308.